Pergamon

Geochimica et Cosmochimica Acta, Vol. 68, No. 18, pp. 3791–3805, 2004

0016-7037/04 $30.00 + .00

doi: 10.1016/j.gca.2004.03.024

Lunar surface geochemistry: Global concentrations of Th, K, and FeO as derived from lunar prospector and Clementine data

JEFFREY J. GILLIS,* BRADLEY L. JOLLIFF, and RANDY L. KOROTEV

Washington University, Department of Earth and Planetary Sciences and the McDonnell Center for the Space Sciences, St. Louis, MO 63130, USA

(*Received February* 5, 2004; *accepted in revised form March* 25, 2004)

Abstract—Accurate estimates of global concentrations of Th, K, and FeO have an important bearing on understanding the bulk chemistry and geologic evolution of the Moon. We present empirical ground-truth calibrations (transformations) for Lunar Prospector gamma-ray spectrometer data (K and Th) and a modified algorithm for deriving FeO concentrations from Clementine spectral reflectance data that incorporates an adjustment for TiO_2 content. The average composition of soil samples for individual landing sites is used as ground-truth for remotely sensed data. Among the Apollo and Luna sites, Apollo 12 and 14 provide controls for the incompatible-element-rich compositions, Apollo 16 and Luna 20 provide controls for the feldspathic and incompatible-element-poor compositions, and Apollo 11, 15, and 17, and Luna 16 and 24 provide controls for Fe-rich compositions. In addition to these Apollo and Luna sample data we include the composition of the feldspathic lunar meteorites as a proxy for the northern farside highlands to extend the range of the calibration points, thus providing an additional anorthositic end-member composition. These empirical ground-truth calibrations for Lunar Prospector Th and K provide self consistency between the existing derived data and lunar-sample data. Clementine spectral-reflectance data are used to construct a TiO_2-sensitive FeO calibration that yields higher FeO concentrations in areas of high-Fe, low-Ti, mare-basalt-rich surfaces than previous FeO algorithms. The data set so derived is consistent with known sample compositions and regolith mixing relationships.

1. INTRODUCTION

We report global surface estimates of K, Th, and FeO using sample data as ground-truth to empirically calibrate Lunar Prospector γ-ray spectrometer (LP-GRS) and Clementine spectral reflectance (CSR) data. We focus on these elements because they (1) are well determined by available global remote sensing data, (2) they are important for determining crustal and whole-Moon compositions and mass balance calculations, (3) their relative and absolute concentrations serve as indicators of different geologic processes, and (4) because of the implications of the distribution of the radioactive elements for lunar internal thermal evolution.

We present empirical calibrations for Th and K concentrations, using the LP-GRS data (Binder, 1998; Lawrence et al., 1998), and FeO concentrations, using the Clementine five-band ultraviolet visible (UVVIS) data (Nozette and The Clementine Team, 1994). We draw a distinction between instrument and empirical calibration; we maintain that once all possible instrumental and environmental factors have been taken into account, the data must then be evaluated on the basis of well-known sample compositions and lunar geochemical relationships, including direct (e.g., Apollo and Luna landing site soil compositions) and indirect ground-truth methods (e.g., comparison to previous remote sensing such as Apollo X-ray and γ-ray, and inference from the compositions of lunar meteorites). Our "recalibration" of these data is an attempt to minimize discrepancies between concentrations calculated using previous calibrations for each of these data sets and sample data. This paper builds upon our preliminary efforts before final release of the LP-GRS data (Gillis et al., 1999, 2000; Haskin et al., 2000).

In the case of the LP-GRS data, the theoretical-physics-based calibration (Lawrence et al., 2000; Prettyman et al., 2002) yields average Th and K concentrations that are systematically high for the Apollo sample data (Fig. 1, Table 1), and relative to the feldspathic lunar meteorites, which we use as a proxy for northern lunar farside highlands (Fig. 2) (Korotev et al., 2003). The LP-GRS data display good precision, but uncertainties of the calibration method have resulted in a systematic overestimation of both elements in previous calibration attempts.

We find that the FeO equation derived from CSR data (Lucey et al., 2000) systematically underpredicts FeO values of low-Ti mare soils (e.g., Apollo 15) as opposed to high-Ti mare soils (e.g., Apollo 17). We present TiO_2-sensitive regression parameters (i.e., slope and offset values in the FeO algorithm) that attempt to account for influence of TiO_2 on the UVVIS spectra. This modification is our attempt to correct for the slight but systematically underestimated FeO values calculated using previous FeO algorithms in locations with low-Ti mare soils. We go on to examine the accuracy of the TiO_2-sensitive FeO equation over a range of FeO and TiO_2 concentrations by comparing calculated and measured FeO concentrations for individual Apollo and Luna soils and comparing the distribution in FeO concentrations calculated for the northern farside feldspathic highlands with the range in FeO concentrations measured in the feldspathic lunar meteorites. This comparison serves as a test of whether the TiO_2-sensitive FeO equation can be applied to the full spectrum of lunar soil compositions. This issue is a concern because of the possibility that the relationship

* Author to whom correspondence should be addressed, at Hawaii Institute of Geophysics and Planetology, University of Hawai'i at Manoa, 1680 East-West Road, POST 504, Honolulu, HI 96822, USA (gillis@higp.hawaii.edu).

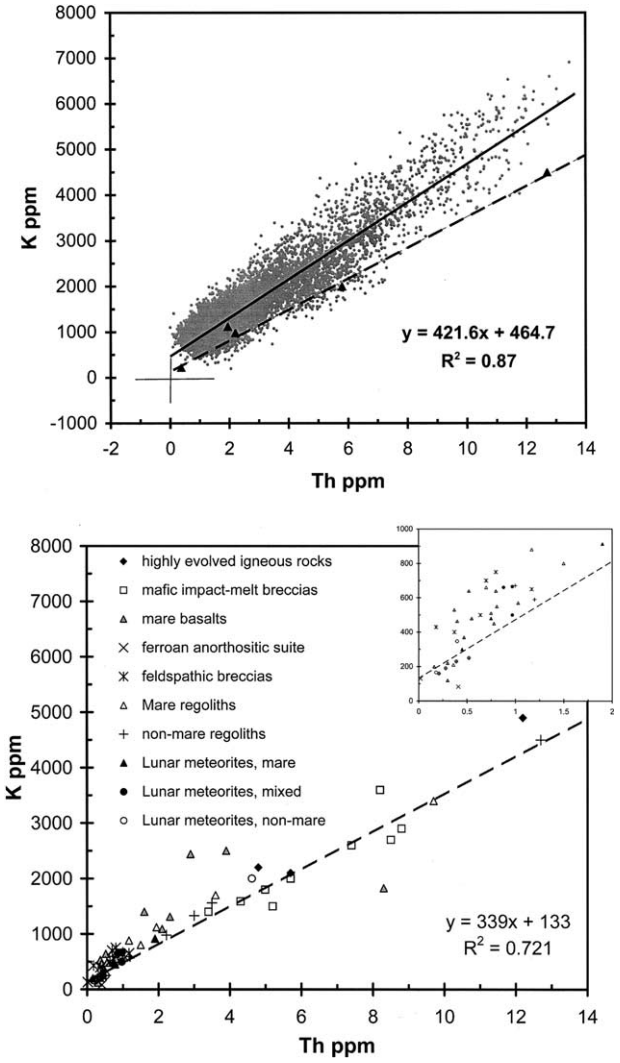

Fig. 1. Variation diagrams (A) K and Th concentrations determined using the Prettyman et al. (2002) and Lawrence et al. (2000) calibrated data. The black line is a best-fit linear regression to the theoretical calibration. The black triangles represent ground-truth data points (Tables 1 and 2), and the dashed line is from (B). Note that the LP-GRS data points tend to lie above the K-Th ratio observed in samples. (B) K with Th concentration data is shown for various lunar materials (data from Korotev, 1998). The diagonal dashed line represents a linear least squares fit to the data for mafic impact-melt-breccia groups, and is the same line as in (A). The inset graph shows the low-Th, low-K data more visibly because the axis range is reduced.

between the Clementine spectral parameter θ_{Fe} (Lawrence et al., 2002), and FeO concentration is nonlinear, and because previous FeO algorithms tended to overestimate the concentration of FeO for the northern farside highlands relative to the feldspathic meteorites.

The method chosen to calibrate all three data sets is a synergistic approach; one that integrates laboratory analyses and remotely sensed data. This method is robust enough to work over the substantial range in scale that the data sets span, from 0.1 km/pixel for CSR to 60 km/pixel for LP-GRS, and for data sets acquired by means of different physical processes. The importance of using ground-truth as a calibration technique has been demonstrated and applied in recent studies (Blewett et al., 1997; Lucey et al., 1998, 2000; Gillis et al., 1999; Jolliff, 1999; Haskin et al., 2000).

Table 1. Site averages of K and Th concentrations in soil used in the ground-truth calibration of the Lunar Prospector gamma-ray data (see Fig. 3).

Regolith	K ± 1σ ppm	Th ± 1σ ppm	K/Th
Apollo 11[a]	1120 ± 30	1.94 ± 0.11	577
Apollo 12[b]	2000 ± 400	5.8 ± 0.27	345
Apollo 14[a]	4500 ± 130	12.7 ± 0.2	354
Apollo 16[a]	980 ± 40	2.2 ± 0.07	445
FLM[c]	220 ± 60	0.37 ± 0.11	595

Feldspathic Lunar Meteorites (FLM). The uncertainties represent the 95% confidence limits based on variations in soil compositions from each of the sample stations.
[a] Korotev (1998).
[b] Korotev et al. (2000).
[c] Korotev et al. (2003).

Lab analyses of soils from the Apollo and Luna landing sites provide comprehensive information about the chemistry, mineralogy, and physical state of the lunar surface of each site. Remotely sensed data, on the other hand, offer less detailed and less precise information than samples, but they allow extrapolation of the sample data to the entire lunar surface. Thus, sample data can place constraints on remotely sensed observations and extend sample data to regional and global scales while providing an improved geologic context for the landing sites.

Remotely sensed data provide information needed to test the long-standing question of whether refractory elements (U, Th, and Al) are enriched in the Moon relative to the Earth. An accurate global determination of FeO concentrations provides important constraints on rock types and regolith mixing, and may be used to estimate Al_2O_3 using the inverse relationship between the two elements, which is well-established on the basis of Apollo and Luna samples (Haskin and Warren, 1991, fig. 8.3). As Th and K (and by correlation U) are naturally radioactive, heat-producing elements, understanding their distribution at the surface and extrapolating their concentrations to depth using geologic and petrologic relationships is vital to understanding thermal evolution of the crust and mantle. These elements provide constraints on the structural-geochemical framework of the Moon. For instance, because K, Th, and Al_2O_3 are so strongly concentrated into the crust (Jolliff et al.,

Table 2. Average K and Th concentrations determined from Lunar Prospector concentration data (2° resolution) for areas used in ground-truth calibration (see Fig. 3).

Remote	K ± 1σ ppm[a]	Th ± 1σ ppm[b]	K/Th	No. pixels
Apollo 11	1739 ± 478	2.98 ± 0.4	584	3
Apollo 12	4376 ± 128	8.1 ± 1.0	540	6
Apollo 14	5836 ± 258	11.2 ± 0.7	521	6
Apollo 16	1900 ± 172	3 ± 0.4	635	6
FHT	858 ± 141	1.0 ± 0.3	825	396

Feldspathic Highlands Terrane (FHT)
[a] Prettyman et al. (2002).
[b] Lawrence et al. (2000).

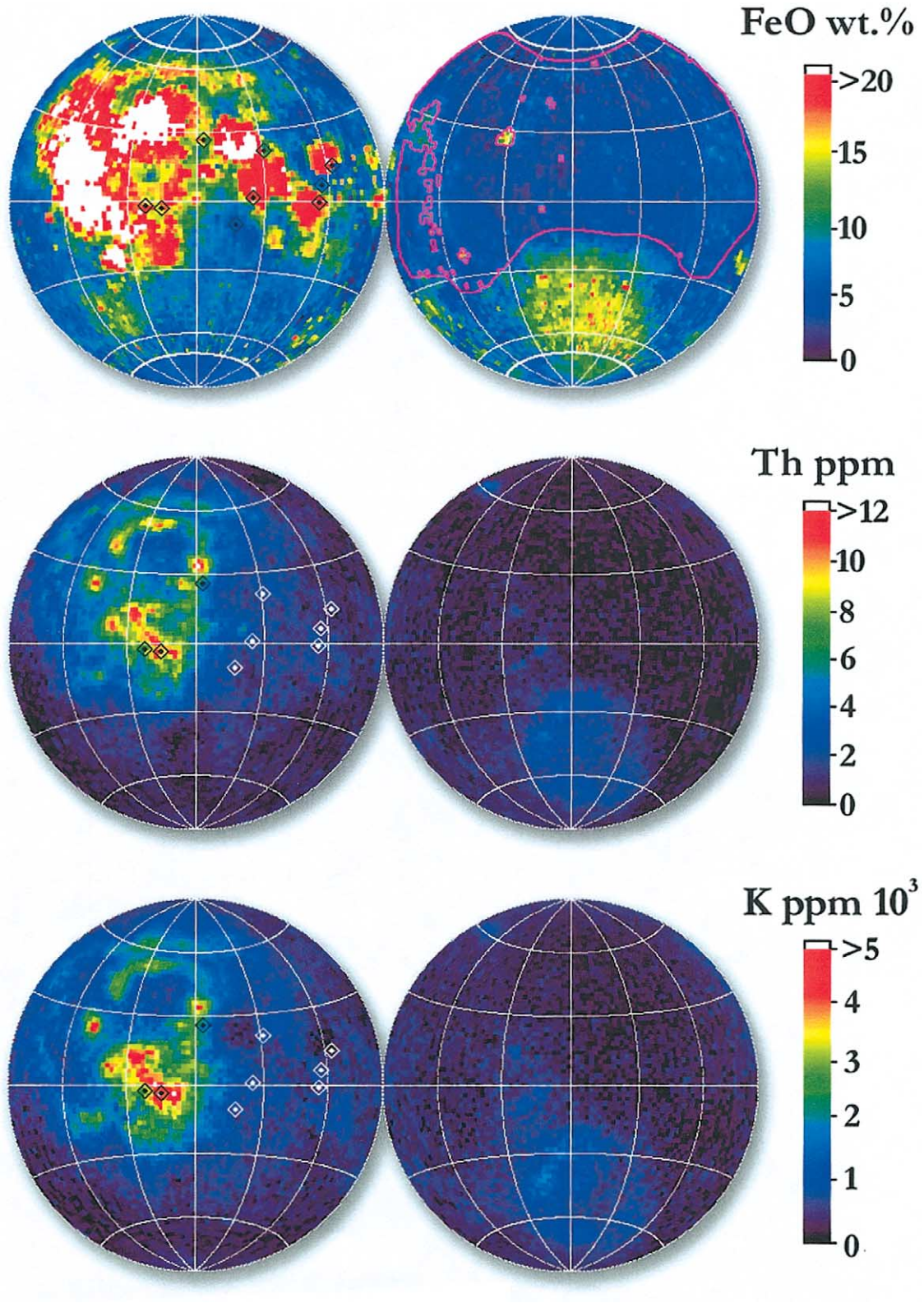

Fig. 2. Lambert equal-area projections showing the distribution of FeO, Th, and K, as determined using the calibrations discussed herein, for the near-side (left) and farside (right) hemispheres of the Moon. Diamonds depict the Apollo and Luna Landing site locations. The latitude and longitude grid spacing is 30°. The region enclosed by the pink outline defines the region of the northern feldspathic highlands from which data were taken for comparison to the feldspathic meteorites and between the different remote-sensing methods. The diamonds represent Apollo (A) and Luna (L) landing sites, from west to east: A12, A14, A15, A16, A11, A17, L16, L20, L24. The heavy white line at 70° north and south in the FeO image represents where Clementine data were supplemented with LP-GRS FeO data because CSR-based FeO data do not extend poleward of 70° owing to extremely high phase angles. None of the supplemented data are included in the statistical calculations discussed in the text.

2000), an accurate determination of their crustal distribution is essential for chemical mass-balance calculations for the bulk Moon as well as for the crust (Taylor and Jakes, 1974; Drake, 1986; Jolliff et al., 2000; Jolliff and Gillis, 2002; Taylor et al., 2002; Warren, 2001). On this basis we present new calibrations for K, Th, and FeO in an attempt to improve the interpretability of the data.

2. EMPIRICAL CALIBRATION OF THE LUNAR PROSPECTOR K AND Th DATA

2.1. Justification for Empirical Calibration

The calibrations of Lawrence et al. (2000) and Prettyman et al. (2002) are based on processes that are involved with creation and detection of γ-rays in the spectral region of the main ^{232}Th γ-ray (2.6 ± 0.1 MeV) and ^{40}K γ-ray (1.4 ± 0.1 MeV). The need for further calibrating the Th data is driven by what we interpret to be inconsistencies in the remotely sensed data relative to sample data. For instance, the correlation between the K and Th concentrations in sample data is strong and well understood in terms of lunar rock compositions and mixing relationships, yet in the remotely sensed γ-ray data, a systematic offset of K/Th of some 20% exists relative to the sample data (Fig. 1). This comparison is made using two separate sample data sets. First is the average composition of representative soils from each of the Apollo landing sites (Tables 1 and 2), which are shown as triangles in Figure 1. Second is the average composition of mafic impact-melt breccias (Fig. 1B). The trend fit to the impact-melt breccias is also a good match to the Th and K compositions of other lunar materials (Fig. 1B) and to the average compositions of the Apollo sites (Fig. 1A). Mafic impact-melt breccias are physical mixtures of rock types produced during basin-forming events. As the lunar surface is a physical mixture of local and regional rock types, we assume that the impact-melt breccias serve as a close approximation for the composition of the lunar surface.

As shown in Figure 1, the LP-GRS Th and K data correlate well and thus appear to have good precision but exhibit a different slope from the sample data. In order for the derived data to be of use for geochemical and petrologic interpretations, such as are possible using lunar-sample data, the remotely sensed data need to be consistent. Without the empirical calibration, these data are unusable for many geochemical purposes, so we are driven to apply a "transform" that yields a data set that is more consistent with the sample data.

An explicit assumption in the Th calibration of Lawrence et al. (2000) is that the pixel with the fewest counts of Th γ-rays contains zero concentration of Th, and that Th abundance scales linearly as the number of counts increases from this zero-point to the maximum count rate. As a result, the mean composition of the northern farside highlands (see Fig. 2 for location) is higher than expected for highly feldspathic soils (~1 ppm Th). This overestimation is because the theory that zero counts equals zero Th abundance does not take into account the uncertainty accompanied by the assumptions that are inherent in the calibration technique (e.g., uncertainty in the detection efficiency and, for nonradioactive elements, uncertainty in neutron absorption cross section, neutron flux, and decay constants), which can amount to uncertainties on the order of 20%. Thus, using the composition of the feldspathic lunar meteorites as a proxy for the Feldspathic Highland Terrane (Jolliff et al., 2000) and composition of averages soils from the Apollo landing sites (Fig. 3), we can justifiably lower the mean Th concentration of the farside to a concentration that is more reasonable compared to the samples, i.e., 0.4 ppm (Table 3).

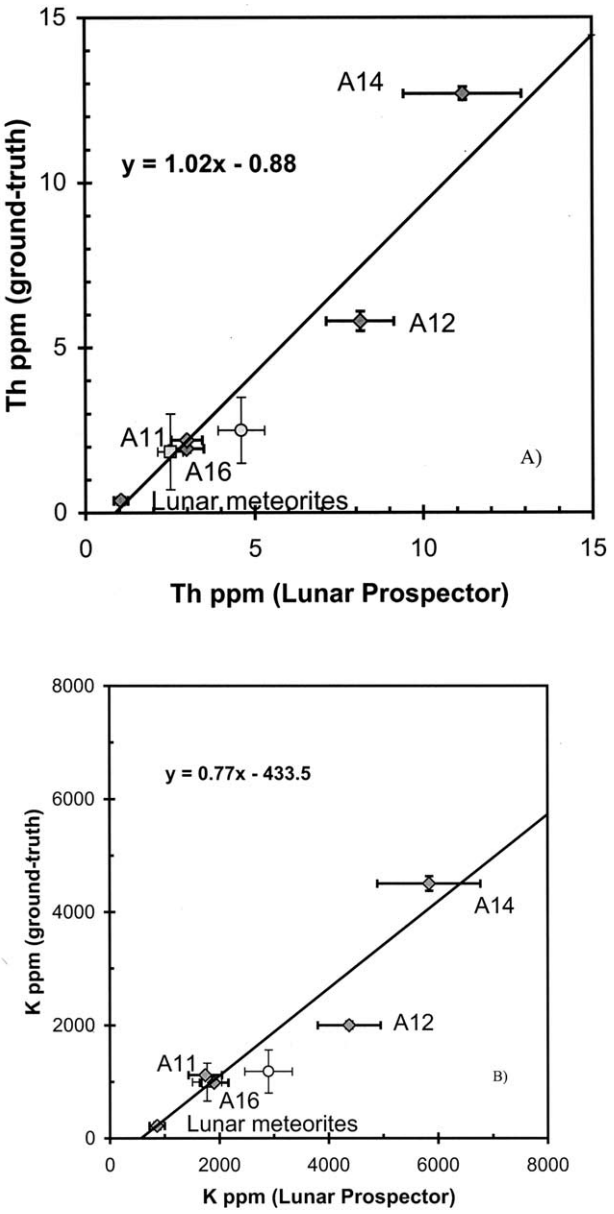

Fig. 3. Th and K concentrations presented for average soil composition for individual landing sites and for the corresponding locations in the Lunar Prospector γ-ray data. The composition of feldspathic lunar meteorites is taken to represent the feldspathic highlands of the northern lunar farside (anorthositic region of the Feldspathic Highlands Terrane). The resulting regression in each plot provides a ground-truth comparison of analyzed and derived compositions, using the theoretical calibration for Th and K (Lawrence et al., 2000; Prettyman et al., 2002), and is subsequently used to transform each data set. Data for the Apollo 15 (gray circle) and 17 (gray square) landing sites are given only as reference and did not contribute to the regression. Compositions for the Apollo 15 and 17 sites are a 50:50 mixture of highland and mare materials. The y-direction error bars for the Apollo 15 and 17 soils denote the min (mare) and max (highlands) data values for Th and K of the two rock types reported by Korotev (1998).

Table 3. Comparison of Clementine-derived FeO and TiO_2 concentrations for 1° and 2° per pixel areas containing an Apollo landing site and average soil compositions collected at the same site.[a]

	FeO ± 1σ	TIO_2 ± 1σ	Min lat	Max lat	Min lon	Max lon
Apollo 12						
Clementine data						
2 degree pixel	16.9 ± 0.9	5.2 ± 1.0	4.0S	2.0S	22.00W	24.00W
1 degree pixel	16.8 ± 0.4	5.0 ± 0.6	3.5S	2.5S	22.75W	23.75W
2 degree pixel	16.4 ± 1.1	4.0 ± 0.9	4.0S	2.0S	20.00W	22.00W
1 degree pixel	16.6 ± 0.5	4.3 ± 0.5	3.5S	2.5S	20.50W	21.50W
2 degree pixel	14.7 ± 2.5	3.1 ± 1.2	4.0S	2.0S	18.00W	20.00W
1 degree pixel	14.9 ± 3.0	3.1 ± 1.0	3.5S	2.5S	18.50W	19.50W
Soil analysis						
Apollo 12	16.5 ± 0.33	2.8 ± 0.05				
Apollo 14						
Clementine data						
2 degree pixel	12.9 ± 0.5	2.0 ± 0.2	4.0S	2.0S	16.00W	18.00W
1 degree pixel	12.9 ± 0.4	1.9 ± 0.2	3.5S	2.5S	16.50W	17.50W
2 degree pixel	12.9 ± 0.6	2.4 ± 0.3	2.0S	0.0	16.00W	18.00W
1 degree pixel	13.0 ± 0.4	2.3 ± 0.2	1.5S	0.5S	16.50W	17.50W
2 degree pixel	13.0 ± 0.4	1.9 ± 0.2	6.0S	4.0S	17.00W	19.00W
1 degree pixel	13.1 ± 0.3	1.9 ± 0.2	5.5S	4.5S	17.50W	18.50W
Soil analysis						
Apollo 14, nonmare	10.5 ± 0.18	1.7 ± 0.05				
Apollo 16						
Clementine data						
2 degree pixel	5.9 ± 0.5	0.9 ± 0.1	9.75S	7.75S	13.75E	15.75E
1 degree pixel	5.9 ± 0.7	0.9 ± 0.1	9.25S	8.25S	14.25E	15.25E
2 degree pixel	5.8 ± 0.7	1.0 ± 0.2	8.25S	6.25S	15.00E	17.00E
1 degree pixel	5.9 ± 0.5	1.1 ± 0.1	7.75S	6.75S	15.50E	16.50E
2 degree pixel	4.9 ± 0.8	0.8 ± 0.2	11.50S	9.50S	15.50E	17.50E
1 degree pixel	5.1 ± 0.7	0.9 ± 0.2	11.00S	10.00S	16.00E	17.00E
soil analysis						
Apollo 16, Cayley Plains	5.5 ± 0.07	0.6 ± 0.013				

[a] The first two rows of Clementine data represent pixels that contain the Apollo landing site. Addi-tional rows of data represent compositional information for areas containing similar geologic units to those observed at the landing sites. Sample data are from Korotev (1998) and Korotev et al. (2000), and uncertainties represent the 95% confidence limits based on sample-to-sample variation. lat = latitude; lon = longitude.

In the case of K, a similar overestimation of K concentration occurs when compared with sample data (Tables 1 and 2), yielding a systematic 20% offset at 6 ppm Th (Fig. 1). The K data, however, were derived from fitting the γ-ray spectrum using a "library least squares" method (Prettyman et al., 2002), thus the assumption that the pixel with the lowest counts is equal to zero K abundance has not been made. The overestimation of K abundance may be due to uncertainties in translating individual γ-ray peaks to elemental concentrations and correctly summing all of the detected major elements (e.g., Si, O, Al, Fe, Mg, and Ti).

The data used in this study were acquired during the low altitude portion of the Lunar Prospector Mission and processed at 2° (60 km) resolution. Although higher-resolution data are available for Th (0.5°), the 2° data were chosen because they permit direct comparison with the 2° K data. Figure 3, illustrates a comparison between Th and K abundances for the mean compositions of soils from the Apollo 12, 14, and 16 landing sites (section 2.2.1) and the feldspathic lunar meteorites (section 2.2.2) versus the Lunar Prospector Th and K concentrations from the theoretical-based calibration as of January, 2002 (Lawrence et al., 2000; Prettyman et al., 2002). We also acknowledge that the LP-GRS data we are using in this paper are an iterative product and that subsequent data releases by the Lunar Prospector Science Team may be more accurate (reduced versions of Lunar Prospector spectrometer data may be available at http://wufs.wustl.edu/missions/lunarp/reduced.htm).

2.2. Empirical Ground-Truth Method for Lunar Prospector

The Th-K ground-truth calibration presented here works on the basis of the comparative method used in many analytical procedures, including, for example, instrumental neutron activation analysis (INAA) (Laul, 1979). In this method the composition of the feldspathic meteorites and soils from the Apollo landing sites serve as standards with known concentrations of Th and K (Table 1), which the LP-GRS measured as it flew over each landing site. As these "standards" are counted under the same irradiation conditions and with the same detector as the "unknowns," which are all locations other than the Apollo landing sites and the Feldspathic Highlands Terrane, a regression fit to the standards can be made that relates LP-GRS elemental concentrations to sample elemental concentrations (γ-ray counts are not directly compared to sample concentrations because the reduced LP-GRS data are expressed in concentration, see last paragraph of Section 2.1). This procedure eliminates any uncertainty in the detection efficiency, and systematic errors in spectral background subtraction, which can easily affect the accuracy in determining the absolute concentration of these elements.

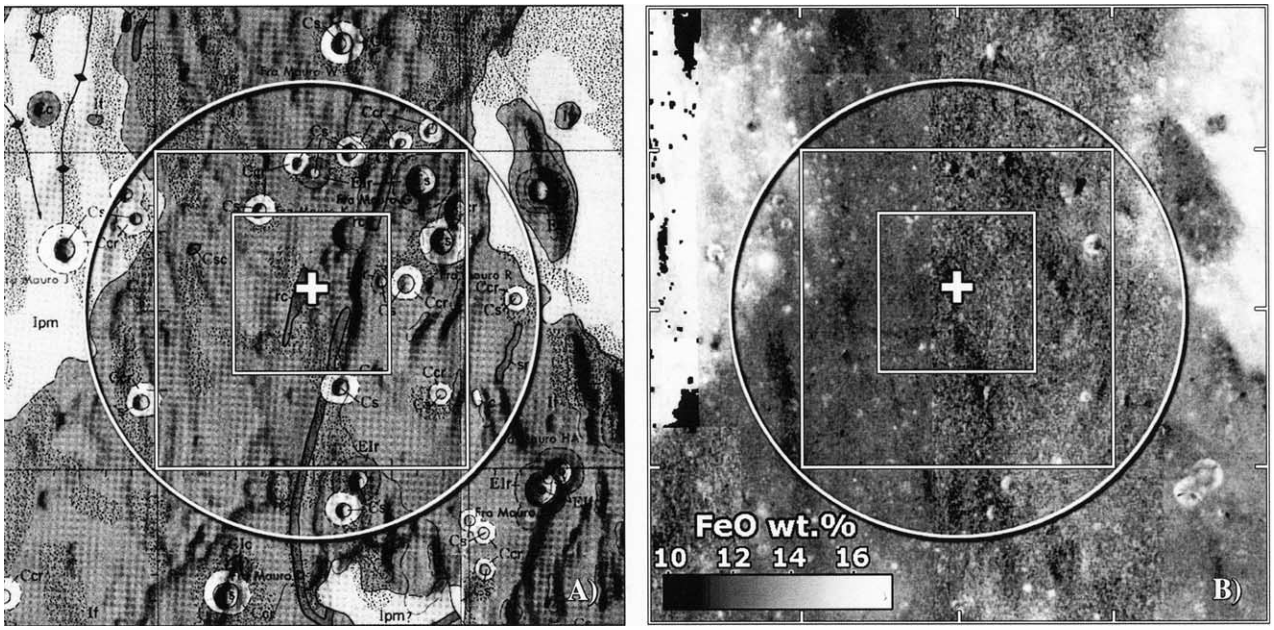

Fig. 4. A) Geologic map of the Apollo 14 landing site "+" (Eggleton and Offield, 1970). The two principal units in this map are the Fra Mauro Formation (darker gray unit mapped as If-Imbrian Furrowed) and mare basalt (lighter gray unit mapped as Ipm-Imbrian plains material). B) Clementine-based FeO image illustrating the variation in FeO composition over the same region, FeO wt% calculated using the algorithm presented herein. The Fra Mauro Formation is dark (average FeO ~12 wt%) and the mare basalts are bright (average FeO ~16 wt%). Both images cover between 15°-19°W, and 1°-5°S in Mercator projection. The smallest square represents a 1° area, and the bigger square represents a 2° area around the landing site. The boxes depict the area where FeO and TiO_2 concentration data were collected, statistically analyzed, and presented in Table 3. Additional data presented in Table 3 for the Apollo 14 landing site comes from adjacent areas north and south of the 2° box shown, and are also composed mostly of Fra Mauro Formation. The circle illustrates the 2° area observed by the Lunar Prospector γ-ray spectrometer.

Here the comparisons are made for Th and K concentrations between Lunar Prospector data and five ground-truth data points (Fig. 3). The resulting regression lines (Eqns. 1 and 2) are derived from a linear least-squares regression to the data where each concentration value is weighted according to its uncertainties (York, 1969).

$$\text{Th ppm} = 1.02 \times \left(\text{LP-GRS Th ppm}\right) - 0.88 \qquad (1)$$

$$\text{K ppm} = 0.77 \times \left(\text{LP-GRS K ppm}\right) - 433.5 \qquad (2)$$

Failure to account for uncertainties in both the X and Y directions yield a linear least squares regression that has greater negative offsets and different slope values (steeper slope for Th and a shallower slope for K). The two regression equations (Eqns. 1 and 2) are then used to transform the LP-GRS data to the values reported here. The distribution of these two elements is shown globally in Figure 2.

2.2.1. Composition of the Apollo landing sites

In this study, we develop empirical calibrations based largely on correlations between the average concentrations of Th and K in soil samples from Apollo landing sites (Korotev, 1998) and the concentrations of these elements in LP-GRS data (Lawrence et al., 2000; Prettyman et al., 2002). Apollo soil data prove useful as calibration points because they span much of the range of Th and K concentrations observed on the lunar surface. Average site compositions were determined by calculating an average of typical <1-mm fines from mature regolith samples (Korotev, 1998, and reference therein; Korotev et al., 2000; Korotev and Gillis, 2001). Samples are weighted in proportion to the magnitude a specific soil sample is assumed to represent an entire site.

For our calibration, we selected Apollo landing sites that exhibit low compositional variation across a 2° area (the resolution of a LP-GRS pixel) to ensure that the comparison between the Th and K concentration of a 2° pixel and the soil concentration of these elements is meaningful (Tables 1 and 2). For that reason we exclude data from Apollo 15 and 17, the two missions for which soil compositions vary greatly across the site because they were located at a mare and highlands boundary. To assess compositional variations over a 2° area surrounding a given landing site we examined FeO and TiO_2 concentrations derived from CSR data (Lucey et al., 2000), calculated at 100 m/pixel resolution (Fig. 4, Table 3). We reason that if a low compositional variation exists in the distribution of both of these oxides over a 2° area then, by inference, Th would also exhibit a restricted compositional range.

We find that the CSR-derived FeO and TiO_2 concentrations for individual pixels at the Apollo 11, 12, 14, and 16 landing sites exhibit little compositional variability over 1° and even 2° areas (±2 wt% deviation in FeO and TiO_2 from their respective means), and are generally similar to the average composition of soil samples from these sites. The

small overprediction of FeO concentration by the CSR calibration (Lucey et al., 2000) relative to the Apollo 14 soil samples is noted. The compositional variation across the Apollo14 site at 2°, however, is among the lowest of all the sites studied, and it is the compositional variation that is of concern. The discrepancy in FeO may be caused by a limitation of the FeO calibration; e.g., difference in mafic mineralogy or glass content relative to soils from the other Apollo sites used in the calibration (Lucey, personal communication, 2001). Thus, Th and K concentrations calculated for Lunar Prospector pixels that include the Apollo 11, 12, 14, and 16 landing sites are then plotted against the average Th composition for these landing sites (Fig. 3, Tables 1 and 2). As noted above, data from the Apollo 15 and 17 missions have been excluded in our regression calculations, although compositions are plotted for reference in Figure 3.

Compositional similarities between the 1° and 2° boxes (Table 3), which are centered within the 2° boxes containing the landing site (Fig. 4), establishes that the variation in FeO and TiO_2 does not significantly change as the area is decreased. Also included in Table 3 are statistics for 1° and 2° areas containing the same geologic unit(s) as the landing site but adjacent to the 2° box containing the landing site. The similarity in composition of these additional boxes with composition of the 2° area that includes the landing site (Table 3), suggests that the composition of landing site is not anomalous. Slight variations in the proportions of the different geologic units that compose a 2° area can be explained by varying the different lithologic components known to exist within the regolith. This variation can be seen in the eastern most pixel at Apollo 12 and 16. In the Apollo 12 region, the eastern most 2° area contains a higher proportion of Fra Mauro Formation (moderate FeO, high Th) at the expense of mare basalt compared to the other areas. In the Apollo 16 region, the eastern most 2° area contains a higher proportion of the Descartes Formation, which is represented by materials from North Ray Crater (Korotev, 1998) as being lower in FeO and Th than the Cayley Plains.

2.2.2. Composition of the feldspathic lunar meteorites

We assume that the average composition of the feldspathic lunar meteorites provides the best estimate of the average composition of the northern farside highlands. This assumption is based on many observations that are reviewed by Korotev et al. (2003), and which are summarized here. (1) None of the regoliths of the Apollo sites are typical of the feldspathic highlands because all contain large proportions of mare volcanics or Th-rich material of the Procellarum KREEP Terrane. (2) Most feldspathic lunar meteorites are breccias composed of regolith. Judging from Apollo regoliths (soils and breccias), we can expect their compositions to represent well the surface of the area from which they each originate (e.g., Warren, 1994). (3) Although we do not know the source location of any of the approximately 16 feldspathic lunar meteorites or the exact number of different locations from which they originate, there are reasons to believe that they derive from small craters representing numerous impacts, perhaps 6 to 16. In other words, they appear to be random samples from several locations. (4) Because of their compositions (low FeO and Th concentrations) and lithologic components (mare volcanics and K- and Th-rich lithologies are rare), most feldspathic lunar meteorites must originate from regions distant from the Procellarum KREEP Terrane and sources of mare volcanic material. (5) Results of Clementine and Lunar Prospector indicate that the northern farside highlands are relatively uniform in composition and have among the lowest concentrations of FeO and Th observed on the Moon (Lucey et al., 1994; Elphic et al., 1998; Jolliff et al., 2000; Lawrence et al., 2001). The inferred composition is qualitatively consistent with the feldspathic lunar meteorites, which are all similar (but not identical) in composition (Fig. 1B). (6) The median distribution of FeO concentrations on the lunar surface as derived from orbit, which corresponds mainly to the vast northern highlands, matches well with the average concentration of FeO in the feldspathic lunar meteorites. On the basis of these observations, our specific assumption is that the mean concentrations of FeO, K, and Th in the feldspathic lunar meteorites (Korotev et al., 2003) are essentially the same as those of the northern farside highlands. This assumption allows us to extend the ground-truth calibration to lower concentrations of all three elements than can be provided by Apollo regoliths because of the proximity of the Apollo sites to the FeO-, K-, and Th-rich Procellarum KREEP Terrane. The reason for including the lunar meteorites in the regression is to serve as anchors at the low-concentration ends of the K, Th, and Fe correlations.

2.3. Ground-Truth Based K and Th Results and Discussion

Comparing Th and K values calculated herein (Fig. 5, darker points) with those from the LP-GRS data (Fig. 5, lighter points) reveals how our empirical calibration translates the Th and K data to lower concentrations. The simple translation that the empirical calibration maintains relative concentrations, i.e., areas where LP-GRS data values were the lowest remained so in our data sets and areas that were high in the previous data sets are still high. These extremes in Th and K concentrations are observed on the northeastern farside (30°N, 150°W; 0 ppm Th; 190 ppm K), the Fra Mauro Formation (11.4 ppm Th; 4340 ppm K), and Aristillus crater (11.4 ppm Th; 3665 ppm K) (Fig. 2).

The most noticeable difference in the translated data is that a small number of negative values exist for both Th and K (Fig. 6). Although negative concentrations are geochemically impossible, we think that they are warranted on the basis of uncertainties in the detection and calibration of the γ-ray data. Therefore we suggest that all negative values should be taken to represent some very low concentration near zero. All statistical calculations herein treat these values as zero concentrations.

The empirical calibration modifies Th concentrations below 2 ppm from the theoretical calibration more than for values greater than 2 ppm. For example, Th values <2 ppm differ by $\sim$85%, while Th values at the high end of the data (13 ppm) experience a difference of only 4%. Consequently, the global surface mean decreases from 2.4 to 1.6 ppm Th and the mode decreases from 1.4 to 0.6 ppm Th (Fig. 6, Table 5). In addition, the average Th value determined for the bulk lunar surface is in good agreement with the estimate calculated by Metzger et al. (1977) of 1.46 ppm Th, which assumes that the composition

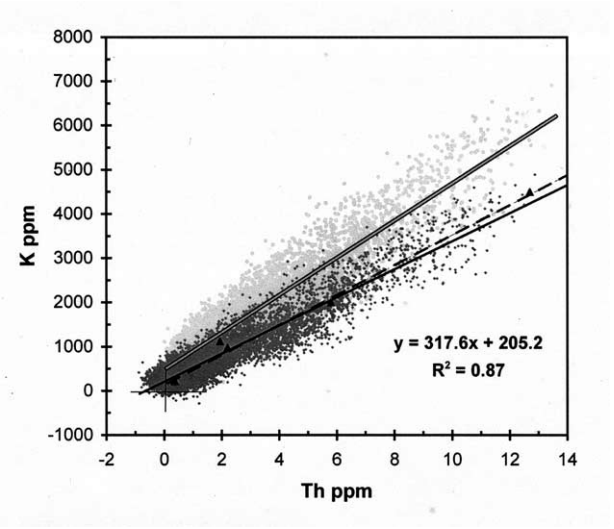

Fig. 5. Variations in concentrations of K and Th are plotted for the ground-truth calibrated Lunar Prospector γ-ray data (dark gray points), with best-fit line to the data (black line). The black triangles represent ground-truth data points (Tables 1 and 2). Compositions from the recalibrated data more closely match the K and Th concentrations of the sample data (Korotev, 1998) (dashed line, Fig. 1B) than K and Th concentrations determined using the theoretical calibration (light gray points which tend to lie above the K-Th ratio observed in samples). The gray line with black outline is a best-fit linear regression to the Prettyman et al. (2002) and Lawrence et al. (2000) calibrated data. The diagonal dashed line represents a linear least squares fit to the mafic impact melt breccia data, and is the same line in Figure 1.

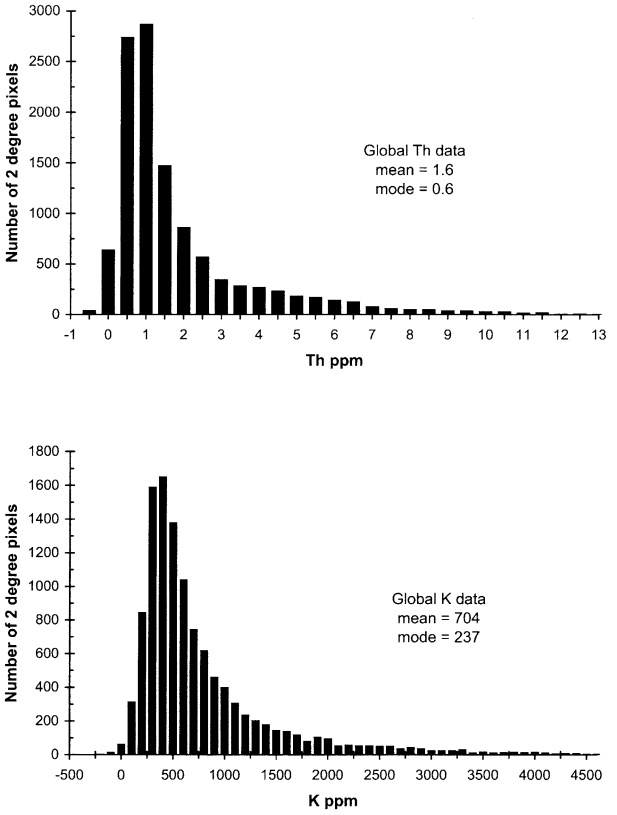

Fig. 6. The statistical distribution of Th and K for the global data set is shown in these two histograms. The compositions have been determined using a ground-truth calibration.

over the whole of South Pole–Aitken Basin is similar to that observed for the Apollo ground tracks near Van de Graaff (2.4 ppm Th).

In the case of the K data, the empirical calibration preferentially lowers the highest K values relative to the lowest (just the opposite of the Th calibration). For instance, values around 1000 ppm K exhibit a difference of 33%, whereas original values around 8000 ppm K show a 72% difference. Consequently, the calculated K concentrations decrease from a global surface mean of 1480 ppm and a mode of 1170 ppm to a mean of 700 and a mode of 240 ppm K (Fig. 6, Table 5). These lower values of bulk surface K are in excellent agreement with those of Metzger et al. (1977), 710 ppm K (the global surface composition that assumes the composition of Van de Graaff to approximate the floor of South Pole–Aitken Basin is 790 ppm K), and 600–700 ppm K from Parker et al. (1981).

Tying the LP-GRS data directly to the lunar sample data yields a data set that reflects the distribution in compositions observed in the sample data. A graph of the transformed Th and K data shows that they closely match the Th and K concentrations (and correlation) of sample data (Fig. 5), as expected. Additionally, the distribution of Th and K concentrations on the lunar surface as derived from ground-truth empirical method compares well with the frequency distribution of the compositions of all of the lunar meteorites (Fig. 7, Tables 1 and 2). This reasoning is admittedly somewhat circular; however, the power of the calibration is that it yields concentration values that are consistent with sample data. Thus, the empirical transformation reconciles inconsistencies between the previous data set and the sample data, and permits greater confidence in the composition of pixels that lie away from ground-truth locations. Accordingly, geochemical and petrologic interpretations similar to those using lunar-sample data can now be made.

The transformed data provide a global distribution of elemental concentrations from which more accurate estimates of the lunar crust and mantle bulk compositions can be made. The data presented here exhibit lower Th values for the Feldspathic Highlands Terrane but higher Th values for the Procellarum KREEP Terrane (Table 4). Coupled with information about crustal structure derived from gravity data (e.g., Wieczorek and Phillips, 1998), surface geology and petrologic relationships can be used to infer compositions at depth as done by Jolliff et al. (2000), and thus to model crustal and global composition (e.g., Jolliff and Gillis, 2002; Taylor et al., 2002). Given that the Feldspathic Highlands Terrane constitutes a major portion of the crust, a difference of 0.5 ppm throughout the Feldspathic Highlands Terrane equates to a 20% difference in the global Th content estimated according to the model of Jolliff et al. (2000). Bulk crustal Th concentrations estimated on the basis of results from this work yield an average crustal concentration (integrated through the depth of the crust) of 0.9 ppm (Jolliff and Gillis, 2002), similar to estimates of Jolliff et al. (2000), Taylor (1982), and Warren (2001).

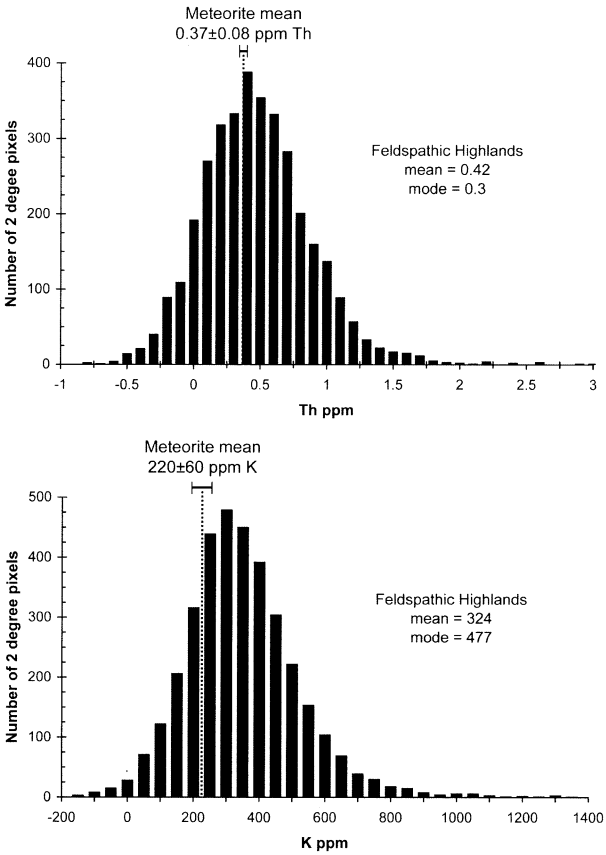

Fig. 7. These histograms illustrate the distribution of Th and K concentrations for the part of the Feldspathic Highlands Terrane located on the northern lunar farside, as depicted in Figure 2. The mean concentration of Th and K determined for the lunar feldspathic meteorites (Korotev et al., 2003) is illustrated for comparison.

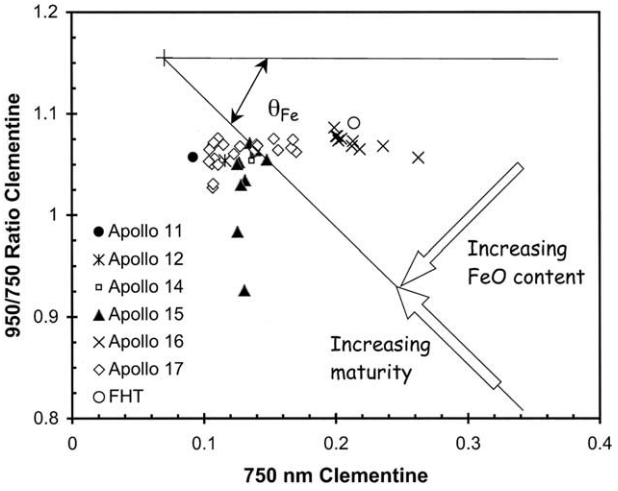

Fig. 8. The spectral parameter θ_{Fe} is determined using a comparison of Clementine 950/750 ratio versus 750 nm. As FeO in the samples increases the value θ_{Fe} increases. Variations in maturity produce trends radial to the origin and counter to compositional trends (θ_{Fe}). Data presented here represent individual pixels (100 m/pixel) that contain separate Apollo and Luna landing sites and sampling stations. The spectrum of the Feldspathic Highlands Terrane (FHT) is also shown.

3. MODIFICATION OF THE CLEMENTINE UVVIS-BASED FeO ALGORITHM

3.1. Justification for Modification

We observe that in areas of high-FeO and low TiO_2 concentrations (e.g., Apollo 15, Luna 24) the method for calculating FeO developed by Lucey et al. (2000) underestimates some FeO concentrations. As shown by Staid and Pieters (2000), the mineralogy that comprises a mare soil affects the spectral trends observed to correspond to FeO concentration (Lucey et al., 1998). Thus we reassess the calibration method of Lucey et al. (2000) in an attempt to improve estimates of FeO calculated from Clementine UVVIS data.

Lucey et al. (1995) developed the first algorithm for calculating the percentage of FeO at the lunar surface using Clementine reflectance data at 750 nm and the ratio of reflectance at 950 nm and 750 nm. This algorithm was based on the observation that the spectral effects of maturity and FeO concentration appear to form opposing spectral trends in laboratory spectra of lunar soils. Improving upon this lab-based algorithm, full-resolution (~100 m/pixel) Clementine images were used to demonstrate that similar opposing trends were observed in remotely sensed spectra (Fig. 8) and the resulting spectral

Table 4. Th and FeO concentrations in crustal terranes (Jolliff et al., 2000) as exposed at the lunar surface.[a]

	Th ± σ, ppm[b]	Th ± σ, ppm This Study	FeO ± σ, wt%[b]	FeO ± σ, wt% (this study)
FHT-An	0.8 ± 0.3	0.5 ± 0.4	4.2 ± 0.5	4.3 ± 1.8
FHT-O	1.5 ± 0.8	1.0 ± 0.7	5.5 ± 1.6	6.4 ± 2.9
Other mare	2.2 ± 0.7	1.6 ± 0.7	16.2 ± 2.3	15.3 ± 2.6
PKT-nonm	5.2 ± 1.4	5.4 ± 1.8	9.0 ± 1.6	10.6 ± 1.8
PKT-mare	4.9 ± 1.0	5.2 ± 1.9	17.3 ± 1.8	17.8 ± 2.2
PKT mixed	4.5 ± 2.0	5.2 ± 1.9	10.7 ± 2.6	16.0 ± 4.3
SPAT-inner	1.9 ± 0.4	2.2 ± 0.5	10.1 ± 2.1	13.3 ± 3.4
SPAT-outer	1.0 ± 0.3	1.0 ± 0.5	5.7 ± 1.1	7.3 ± 2.8

[a] FHT, Feldspathic Highlands Terrane (An, anorthositic; O, outer, mainly areas outside the northern farside highlands and not included in other terranes); other mare refers to mare deposits located in the FHT, both An and O, for which individual 2 pixels consist entirely of basalt; PKT, Procellarum KREEP Terrane (nonm, nonmare); SPAT, South Pole–Aitken Terrane (inner refers to inside the topographic rim, and outer refers to the area immediately outside the topographic rim).

[b] Th and FeO data presented in table 1 of Jolliff et al. (2000).

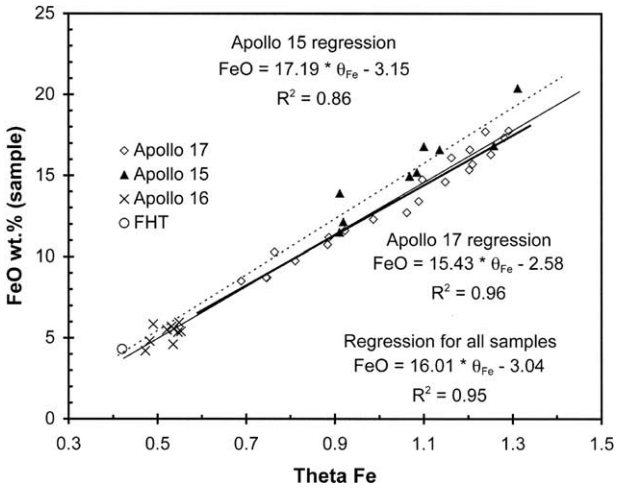

Fig. 9. A linear correlation is exhibited between sample FeO concentration and the spectral parameter θ_{Fe} for individual Apollo 15, 16, and 17 sample stations. The bold line (and the shortest of the three lines) represents a regression fit to all sample stations, the upper dotted line is a regression line fit only to the Apollo 15 sample stations (black triangles) and the lower thin line is a regression line fit only to the Apollo 17 sample stations (gray diamonds). Both the Apollo 15 and 17-regression lines trend through the Apollo 16 soils (×s) and the Feldspathic Highland Terrane (open circle), which was determined using the spectral properties of the Feldspathic Highland Terrane and the mean composition of the lunar feldspathic meteorites. Notice that the regression to all points and to the high-TiO_2 Apollo 17 soils are nearly identical, whereas the trend line to the Apollo 15 low-TiO_2 soils is slightly higher. This difference in slope translates into a difference of–absolute wt% FeO at the high θ_{Fe} end.

parameter, θ_{Fe} (Fig. 9), was then calibrated using ground-truth data (Blewett et al., 1997; Lucey et al., 1998, 2000). The resulting ground-truth calibration yielded a high degree of correlation between the spectral parameter θ_{Fe}, calculated from Clementine images of the Apollo and Luna landing sites, and the average soil FeO concentrations from each corresponding sample station. This method employs a single regression trend using data from all of the landing sites to relate soil FeO concentrations to θ_{Fe}. Consequently, the FeO calibration possesses a bias towards the soil compositions from the Apollo 15 and Apollo 17 sites because these sites bear the majority of sample stations that could be distinguished in Clementine images (and station soils correlated to individual multispectral pixels in the Clementine images) and because soils from these sites have compositions that extend to high-FeO concentrations. The Apollo 17 sample stations alone account for nearly half of the calibration points.

A close look at the data used for the regression shows that data points for Apollo 15 and Apollo 17 lie along two closely parallel but separate lines (Fig. 9). The main chemical (and mineralogical) difference between the two sets is TiO_2 concentration (and ilmenite content); the Apollo 15 basalt component is low in TiO_2 whereas the Apollo 17 basalt component is high in TiO_2. Because ilmenite contains a significant amount of the FeO and does not produce a 1-μm absorption equivalent to that produced by the mafic silicates, it seems likely that the difference between the two sets of data in Figure 9 is related to TiO_2 content. The FeO algorithm has a built-in compensation for the presence of ilmenite. As FeO increases in a soil a spectrum will move in a clockwise rotation lowering in reflectance while increasing in the 950/750 ratio (Fig. 8). Ilmenite, however, because it is spectrally dark and neutral, lowers a soil's UVVIS reflectance and diminishes the mafic absorption of iron silicates at 1-μm. Thus, as ilmenite is added to a soil, it will darken the reflectance but decrease the 950/750 ratio, and as a result the spectra will move toward the origin similar to a maturity trend. On this basis, we modify the "average" regression method by incorporating a term for the TiO_2-content. Previous versions of the FeO algorithm have not attempted to address all possible minor causes of uncertainty. In our judgment, one of the factors that can potentially be taken into account is the TiO_2 content, which varies strongly in the maria. Our adjustment assumes that TiO_2 is contained predominantly in ilmenite and leads to a linear darkening with increasing concentration. We acknowledge that this correction is only provisional, and a more rigorous correction would need to account for TiO_2 in pyroxene, other non-Ti bearing opaques (because non-Ti bearing opaques such as spinels mimic the spectral characteristics of ilmenite but do not contain TiO_2), as well as the various grain sizes and morphologies of ilmenite. Other corrections will be needed for locations such as Apollo 14, South Pole–Aitken basin (where the mafic mineral proportion differ significantly from those in the bulk of the ground-truth regolith samples), and to account for the observation that maria of a given composition may be weathering along parallel trends in the parameter space rather than along rotation lines (Staid and Pieters, 2000).

3.2. Empirical Ground-Truth Method for Clementine UVVIS Data

The method for calculating the FeO regression parameters as presented here is a three-step process, the first two being similar to the method of (Lucey et al., 2000). The first step is to acquire spectral information for individual Apollo and Luna landing sites and sampling stations using single pixel Clementine 100 m/pixel UVVIS data processed with the latest radiometric calibrations and photometric normalizations (McEwen et al., 1998; Eliason et al., 1999a,b). Next, the Clementine UVVIS data are compared on a plot of the 950/750 nm ratio versus reflectance at 750 nm and the angle θ_{Fe} is measured (Fig. 8). The θ_{Fe} parameter is the angle between a line parallel to the x-axis at constant UV/VIS value ($R_{950}/R_{750} = y_{0Fe}$) and a line rotated clockwise from the horizontal to a data point. This technique suppresses effects caused by soil maturity (darkening, reddening, and loss of spectral contrast) so that as the concentration of Fe-bearing silicates in a soil increases, θ_{Fe} increases. Conversely, soils of similar FeO concentrations but differing maturity levels tend to lie along a single line with the same θ_{Fe}, with the more mature soils lying closer to the theoretical "hypermature" or "optimized" origin (x_{0Fe}, y_{0Fe}). The location of the optimized origin used in our regression was determined by maximizing the quality of the second-order polynomial fit between values of θ_{Fe} and sampling station FeO concentrations. These coordinates ($x_0 = 0.07$, $y_0 = 1.155$) differ only slightly from those used by Lucey et al. (2000) ($x_0 = 0.08$, $y_0 = 1.19$), and were chosen to optimize the suppression of maturity effects as well as to maximize the fit to the compositional data. In the third step, θ_{Fe} values are plotted against soil FeO concentrations measured in the laboratory to

Table 5. Comparisons between CSR-based and LP-GRS-based determinations of FeO, Th, and K.[a]

Method	Global mode FeO	Farside mean FeO
Lucey et al. 1995	3.9	
Lucey et al. 1998	7.0	5.5
Lucey et al. 2000	5.8	4.5
Lawrence et al. 2002	5.7	5.1
LP-GRS	4.7	4.3
This study	5.7	4.4
	Th	Th
LP-GRS	1.4	1.0
This study	0.6	0.4
	K	K
LP-GRS	1172	861
This study	424	324

[a] The global mode represents the whole lunar surface between 70°S and 70°N, whereas farside mean is only for the northern farside. All data are resampled to 2° per pixel resolution.

yield a relation that transforms θ_{Fe} into absolute FeO concentrations (Fig. 9, Eqn. 3). Soil compositions are the same as those used by Blewett et al. (1997) and are listed in Table 6.

$$\text{FeO wt\%} = m \times \theta_{Fe} + b \quad (3)$$

$$m = -0.2208 \times TiO_2 + 17.634 \quad (4)$$

$$b = 0.0712 \times TiO_2 - 3.288 \quad (5)$$

The slope and offset of the regression curve were determined as a function of the concentration of TiO_2, (Eqns. 4 and 5) where the TiO_2 concentration was calculated using Clementine UV-VIS data and the method of (Gillis et al., 2003). These TiO_2-sensitive regression parameters yield lower slopes for higher values of TiO_2—i.e., lower FeO concentrations—than soils with lower TiO_2 contents, and the two trends converge toward compositions of the Apollo 16 soils. Consequently, the TiO_2-adjusted regression method yields higher FeO concentrations than the "average-regression" FeO algorithm by 2–3 absolute percent for soils with low TiO_2 concentrations, and produces a better fit to low-Ti, high-Fe soils like those at the Apollo 15 site (Tables 5 and 6).

The feldspathic lunar meteorites, though compared to remotely sensed data for the Feldspathic Highlands Terrane (Table 7), were not used to calibrate the TiO_2-sensitive FeO equation (presented here) because their FeO concentrations are similar to those of Apollo 16 soils, with only ~0.5 FeO wt% difference. This was not the case for the Th and K ground-truth empirical calibration presented earlier (Section 2.2), where the difference in composition between Apollo 16 and the lunar meteorites (1.8 ppm Th, and 760 for K; Table 2) is a significant portion of the total range measured for each element. The difference in composition between Apollo 16 soils and the lunar meteorites is 15 and 16% of the total range for Th and K respectively, but <3% of the range for FeO. Thus, the feldspathic lunar meteorites and remotely sensed data from the Feldspathic Highlands Terrane may be used to assess the accuracy of our new algorithm at low FeO concentrations.

3.3. Comparing Different Estimates of Global FeO Distributions

The FeO data sets that we compare are those from the TiO_2-sensitive FeO equation, the latest CSR-derived FeO equation of Lawrence et al. (2002), which will be referred to as the linearized CSR algorithm, and the LP-GRS values of Prettyman et al. (2002). Comparing the global histograms of FeO highlights the similarities and differences in the statistical distribution of FeO values between the three separate data sets and, in addition, reveals some problems (Fig. 10).

The three histograms are similar at low-FeO concentrations and they share similar global averages and modes, to within a weight percent. The higher FeO values obtained using the TiO_2-adjusted regression algorithm for FeO-rich and TiO_2-poor mare regions, however, are not as high as FeO values obtained by Lawrence et al. (2002) using "linearized" CSR data or FeO concentrations obtained from LP-GRS data (Prettyman et al., 2002). Concentrations of FeO at the high end of the LP-GRS histogram are higher, i.e., greater than 22 wt%, relative to what is expected on the basis of known samples and mixing relationships between mare and nonmare materials in lunar regolith. For example, among the Apollo samples, the most basalt-rich soils only reach 20 wt% FeO even in ejecta of fresh craters, despite the presence of basalt groups whose average FeO concentrations are as high as 2–2 wt% (Basaltic Volcanism Study Project, 1981; Korotev, 1998). Not only do the extremely high FeO values in the LP-GRS data set exceed those expected on the basis of sample data, but petrologic modeling and basaltic phase equilibria also do not support the existence of extensive regions (e.g., at a scale of resolution of 60 km or greater) of mare basalts with FeO concentrations above ~22 wt%.

The histogram for the TiO_2-adjusted FeO values exhibits a broader width of the main low-FeO gaussian distribution. The breadth of this peak at low-FeO concentrations may in part stem from the uncertainty at low FeO concentrations owing to the low signal/noise of what is a weak spectral feature, especially in mature soils, or possibly unidentified mineralogical differences that are not accounted for in the CSR-based FeO calibration. A similar broad distribution at low FeO values was also seen in earlier versions of global data determined using the CSR-based method (e.g., Lucey et al., 2000). The linearized CSR FeO algorithm implements a possible solution to this problem by correlating the CSR data with the LP-GRS count data and then applying a transformation to linearize the correlation (Lawrence et al., 2002). The nonlinear relationship is most pronounced where CSR-based FeO values are <6 wt% or >16 wt%. This transformation effectively stretches the CSR FeO concentrations to more extreme values. Perhaps such a transformation may be an acceptable method to "adjust" the CSR-derived FeO data for determining accurately FeO variations at high spatial resolution, but not until the LP-GRS data are fully validated and shown to be sufficiently accurate at extreme FeO concentrations.

To examine the extent of the nonlinear relationship between CSR and LP-GRS-derived FeO at low FeO concentrations, we compare the distributions of FeO concentrations for northern farside highlands (Fig. 2) for the three FeO algorithms: TiO_2-adjusted, linearized CSR, and LP-GRS (Fig. 11). All three histo-

Table 7. Average FeO, Al_2O_3, Th, and K concentrations measured for the lunar feldspathic meteorites (Korotev et al., 2003) and estimated for northern farside highlands (NFH) using the ground-truth empirical calibration method for Clementine (FeO) and LP-GRS (Th and K) data.

	Meteorite mean	NFH mean	Unit
Al_2O_3	28.2 ± 1.0	27.9[a]	wt%
FeO	4.4 ± 0.5	4.4 ± 1.2	wt%
Th	0.37 ± 0.11	0.4 ± 0.4	ppm
K	220 ± 60	324 ± 173	ppm

[a] For the NFH, Al_2O_3 is calculated using an approximation ($Al_2O_3 = -2.1 \times FeO + 37$) based on the anticorrelation between FeO and Al_2O_3 concentrations observed in sample chemistry.

grams show a normal distribution and are relatively unskewed, as suggested by the similar values for the means and modes of the data. The FeO data for the TiO_2-adjusted regression exhibit a mode ~4.5 wt% FeO for the northern farside highlands, which matches the mode of the feldspathic meteorites and the LP-GRS data. The mean and mode calculated from the linearized Clementine algorithm are shifted towards slightly higher FeO values. We interpret the similarity in the mean and mode between the Clementine TiO_2-adjusted FeO algorithm, the LP-GRS FeO values, and the feldspathic lunar meteorites to indicate that the FeO concentrations derived from CSR data are accurate to first order. Moreover, the TiO_2-adjusted regression produces concentrations (e.g., mean and mode) for the northern farside highlands that are more consistent with the feldspathic meteorite compositions than the Lawrence et al. (2002) and Lucey et al. (1995, 1998) FeO calibrations for CSR data (Table 5).

3.4. TiO_2-Sensitive FeO Equation Results and Discussion

The spectral parameter θ_{Fe} computed for the northern Feldspathic Highlands Terrane (area shown in Fig. 2) and the average FeO value of the feldspathic lunar meteorites (Table 2) are also consistent with the landing-site ground-truth data. The average θ_{Fe} for the northern feldspathic highlands is plotted against the average FeO concentration of the feldspathic meteorites as shown in Figure 9 along with the θ_{Fe} values and FeO concentrations of soils from the Apollo 15, 16, and 17 sites. The average θ_{Fe} value of the northern feldspathic highlands and FeO concentration of the feldspathic lunar meteorites lies along the projection of Apollo 15 and 17 regression lines, just to the left of the Apollo 16 data.

The TiO_2-adjusted regression algorithm provides an accurate means of estimating FeO concentration using Clementine UVVIS data. First, this method yields FeO values that are more consistent with low-Ti mare basalt samples than previous FeO algorithms (Table 6). Secondly, global minimum and maximum FeO values are consistent with chemical and petrological information obtained from lunar samples. Thirdly, the statistical mode and average FeO content of the feldspathic lunar highlands, as determined by the TiO_2-adjusted method, are similar to the mode and average FeO content of the feldspathic lunar meteorites (Fig. 11). In addition, our estimate for the mean composition of the feldspathic highlands (27.9 wt% Al_2O_3; Table 7), where Al_2O_3 is calculated using an approximation based on the anticorrelation between FeO and Al_2O_3 concentrations observed in sample chemistry, is similar to that of Korotev et al. (2003), but slightly more feldspathic than that of Palme et al. (1991; 26.1 wt% Al_2O_3). Finally, the average θ_{Fe} value computed from Clementine UVVIS data of the northern farside highlands and the average FeO value measured for the feldspathic lunar meteorites exhibit a correlation that is similar to the θ_{Fe} and FeO concentrations determined for Apollo soil samples (Fig. 9). Thus, providing useful information for calibrating remotely sensed data. The global distribution of FeO concentrations, according to the TiO_2-adjusted regression algorithm, is shown in Figures 2 and 10.

These revised data for FeO exhibit similar values to those reported by Jolliff et al. (2000) for defining various lunar terranes (Table 4), which used the FeO map derived from Clementine UVVIS data by Lucey et al. (1998). The biggest differences occur in the South Pole–Aitken Terrane and the Procellarum KREEP Terrane, where the Ti-adjusted algorithm reports higher FeO values. These differences could reflect a

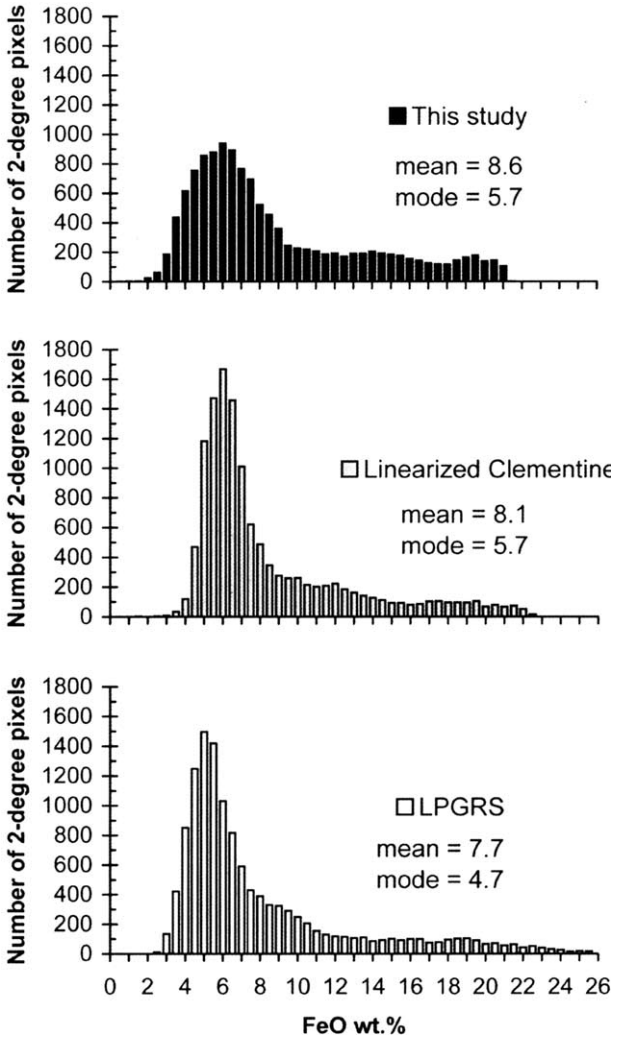

Fig. 10. These three histograms illustrate the global distribution of FeO at 2° resolution (60 × 60 km), between the latitudes of 70° south and 70° north. The first two histograms are based on CSR data (using the algorithm developed herein and the linearized Clementine data of Lawrence et al. (2002) and the lowermost histogram is constructed from LP-GRS data for iron (Lawrence et al., 2002).

Table 6. Comparison of FeO concentrations determined from laboratory analy-sis (FeO meas) and Clementine spectral-reflectance measurements. Clementine FeO data presented were calculated using the TiO_2-adjusted (TiO_2-adj), LP-GRS linearized Clementine, and Lucey et al. (2000) algorithms.

Sample site	FeO meas	FeO calc TIO_2-adj	% deviation	FeO calc linear	% deviation	FeO calc Lucey'00	% deviation
A11	15.8	18.8	19.2	19.3	22.0	18.3	15.6
A12	15.4	17.8	15.7	16.8	9.4	16.1	4.4
A14-LM	10.3	14.0	35.5	12.1	17.7	13.0	26.0
A14-cone	10.7	13.3	24.0	11.6	8.1	12.5	17.3
A15-LM	15.0	15.2	1.8	13.4	10.2	14.1	5.6
A15-S1	16.8	15.8	5.8	14.0	16.9	14.2	15.2
A15-S2	11.5	12.6	9.5	10.8	5.7	11.7	1.7
A15-S4	16.6	16.5	0.6	14.7	11.6	14.7	11.4
A15-S6	12.1	12.7	4.7	11.1	8.7	12.1	0.2
A15-S7	13.9	12.6	9.1	11.1	20.3	12.3	11.8
A15-S8	15.2	15.5	2.3	13.7	9.8	14.3	5.7
A15-S9	16.9	18.5	9.8	17.7	5.1	16.0	4.9
A15-S9a	20.4	19.4	4.9	19.6	3.8	16.5	19.1
A16-LM	5.6	6.1	10.7	6.1	10.6	5.5	0.3
A16-S1	5.4	6.4	19.0	6.3	15.8	5.7	5.7
A16-S2	5.5	5.9	6.7	5.8	5.9	5.0	9.0
A16-S4	4.6	6.1	33.2	6.1	32.0	5.4	17.7
A16-S5	5.9	5.3	8.9	5.8	1.5	4.9	15.7
A16-S6	6.0	6.3	6.7	6.1	2.2	5.4	9.1
A16-S8	5.4	6.3	17.9	6.0	11.9	5.2	1.9
A16-S9	5.7	6.1	6.3	6.1	6.7	5.4	4.5
A16-S11	4.2	5.0	19.8	4.9	16.5	3.4	18.2
A16-S13	4.8	5.2	8.3	5.2	8.9	4.0	16.7
A17-LM	16.6	16.3	1.9	16.0	3.5	16.2	2.4
A17-S1	17.8	17.4	1.9	18.3	2.9	17.0	4.4
A17-S2	8.7	9.7	11.8	8.6	1.4	9.1	4.3
A17-S3	8.7	9.7	11.1	8.6	0.9	9.2	5.5
A17-S5	17.7	16.5	6.5	16.8	5.1	16.6	6.3
A17-S6	10.7	11.9	10.7	10.7	0.7	11.7	9.5
A17-S7	11.6	12.5	7.5	11.1	3.8	12.2	5.2
A17-S8	12.3	13.5	9.7	12.2	0.9	13.3	8.4
A17-S9	15.4	16.7	8.5	16.0	4.4	16.0	4.5
A17-LRV1	16.3	17.1	5.1	17.0	4.6	16.8	3.1
A17-LRV2	13.4	15.2	13.1	13.9	3.4	14.9	11.2
A17-LRV3	14.8	15.1	2.4	14.0	4.9	15.2	3.2
A17-LRV4/S2a	8.5	8.8	3.0	8.1	5.2	8.5	0.2
A17-LRV5	9.8	10.7	10.1	9.5	2.4	10.3	5.7
A17-LRV6	10.3	9.9	3.5	9.1	11.8	9.9	3.7
A17-LRV7	16.1	15.9	1.1	15.2	5.8	15.9	0.9
A17-LRV8	15.7	16.7	6.7	16.1	2.5	16.5	5.0
A17-LRV9	14.6	15.8	8.4	14.9	2.1	15.8	8.3
A17-LRV10	11.2	11.9	6.2	10.7	4.6	11.7	5.0
A17-LRV11	12.7	14.7	15.7	13.4	5.2	14.2	12.2
A17-LRV12	17.4	17.2	0.9	18.0	3.6	16.9	2.7
L16	16.7	18.2	9.1	17.1	2.5	17.1	2.4
L20	7.5	9.2	22.7	8.5	13.7	9.3	23.4
L24	19.5	19.2	1.7	18.0	7.7	17.1	12.3

presence of low-Ti mare and high-FeO nonmare materials that were reported as systematically low in the previous FeO algorithm.

5. CONCLUSIONS

We have attempted to provide "final" empirical calibrations or "transformations" for Th and K lunar surface concentrations, using the Lunar LP-GRS data, and FeO concentrations, using the CSR data. The resulting global compositional data sets are internally consistent and are consistent with concentrations and correlations present in the sample database. These improvements demonstrate fundamental utility of ground-truth and their importance in the empirical calibration of remotely sensed data.

The ground-truth calibrations for Th and K produce lower concentrations of these elements and better agreement with soil sample analysis than those previously reported. Results from this work may have important implications on interpreting local and regional geology. For example, having accurate Th concentrations is important for modelling the distribution of Th-rich Imbrium antipodal ejecta within South Pole-Aitken Basin (Haskin et al., 1999), and the characterization of surface geology by geochemical unmixing of LP-GRS Th data using compositions of known lithologic materials (e.g., Blewett and Hawke, 2001; Chevrel et al., 2002). In addition, theories of

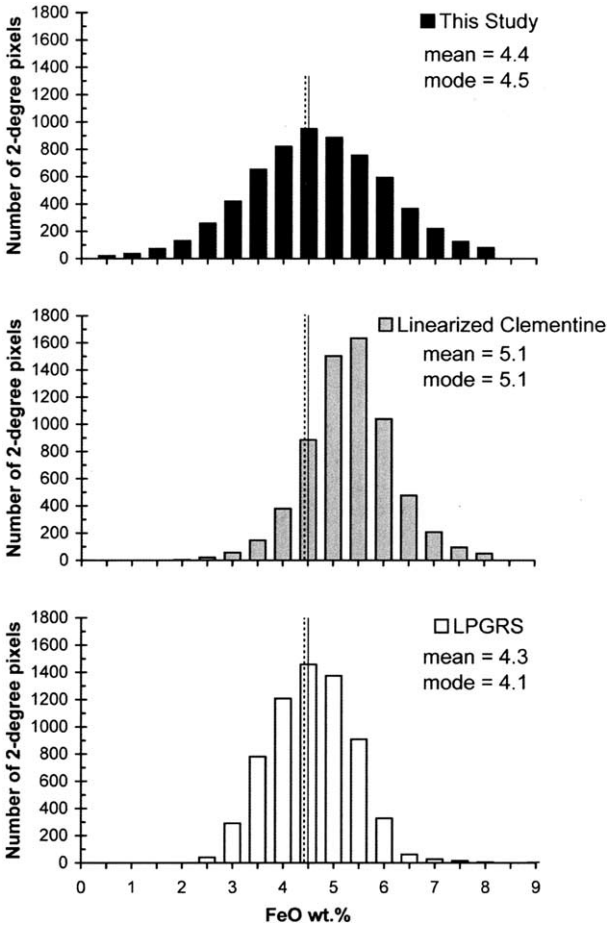

Fig. 11. These three histograms show FeO distribution for the northern feldspathic highlands, at 2° per pixel resolution (60 × 60 km) (see Fig. 2 for subset area). The CSR-based FeO data are presented in the first two histograms (using the algorithm developed herein and the linearized Clementine data of Lawrence et al. (2002) and the third histogram displays the LP-GRS data for iron (Lawrence et al., 2002). The solid line represents the mode of the TiO_2-sensitive algorithm and the dotted line represents the mean of the feldspathic meteorites.

lunar origin, crustal formation (Wood et al., 1970; Longhi and Ashwal, 1985), the three dimensional composition of the crust (Toksöz et al., 1972; Jolliff et al., 2000; Wieczorek and Zuber, 2001), and unraveling the bulk composition of refractory elements in the Moon (Taylor and Jakes, 1974; Ringwood, 1976; Warren and Wasson, 1979; Hood and Jones, 1987; Jolliff and Gillis, 2002; Taylor et al., 2002) may also be addressed. These results emphasize the need for ground-truth validation/calibration/transformation of data sets to account for unanticipated sources of uncertainty or those that are difficult to quantify.

The modified FeO algorithm implements a small adjustment to account for effect of TiO_2 in ilmenite on the UVVIS spectra of basalts. The TiO_2-sensitive FeO derivation using CSR data yields FeO concentrations that more accurately match high-Fe/low-Ti mare-basalt-rich surfaces. The slightly higher FeO contents produced using this algorithm are important for remote sensing studies of basalts with similar high-FeO low-TiO_2 compositions (e.g., Gillis and Spudis, 2000; Blewett and Hawke, 2001). Also, the modified algorithm produces FeO concentrations for the northern farside highlands that are consistent with the feldspathic meteorite compositions (Table 7).

Acknowledgments—Support for this work came from NASA Grants NAG5-8905 and NAG5-10227 (blj). We would like to thank Paul Lucey, David Lawrence, Rick Elphic, Tom Prettyman, and Dave Vaniman for discussions regarding these data sets. Comments and suggestions provided by Matt Staid, G. Jeffrey Taylor, and an anonymous reviewer served to improve this paper and are greatly appreciated.

Associate editor: C. R. Neal

REFERENCES

Basaltic Volcanism Study Project. (1981) *Basaltic Volcanism on the Terrestrial Planets.* Pergamon Press.

Binder A. B. (1998) Lunar Prospector: Overview. *Science* **281,** 1475–1476.

Blewett D. T., Lucey P. G., Hawke B. R., and Jolliff B. L. (1997) Clementine images of the lunar sample-return stations: Refinement of FeO and TiO_2 mapping techniques. *J. Geophys. Res.* **102,** 16319–16325.

Blewett D. T. and Hawke B. R. (2001) Remote sensing and geological studies of the Hadley-Apennine region of the Moon. *Meteor. Planet. Sci.* **36**(*5*), 701–730.

Drake M. J. (1986) Is lunar bulk material similar to Earth's mantle? In *Origin of the Moon* (eds. W. K. Hartmann, R. J. Phillips, and G. J. Taylor), pp. 105–124. Lunar and Planetary Institute.

Drake M. J. (1986) Is lunar bulk material similar to Earth's mantle? In *Origin of the Moon* (eds. W. K. Hartmann, R. J. Phillips, and G. J. Taylor), pp. 105–124. Lunar and Planetary Institute.

Eggleton R. E. and Offield T. W. (1970) Geologic map of the Fra Mauro region of the Moon: Apollo 14 pre-mission map. In *Miscellaneous Geologic Investigations,* USGS Map I-708, 2 sheets. U.S. Geological Survey.

Eliason E. M., Isbell C., Lee E., Becker T., Gaddis L., McEwen A., and Robinson M. S. (1999a) Mission to the Moon: The Clementine UVVIS global images. 78 CD-ROM set produced by the U.S. Geol. Surv., Flagstaff, AZ.

Eliason E. M., McEwen A. S., Robinson M. S., Lee E. M., Becker T. L., Gaddis L., Weller L. A., Isbell C. E., Shinaman J. R., Duxbury T., and Malaret E. (1999b) Clementine: A global multispectral map of the Moon from the Clementine UVVIS imaging instrument. *Lunar Planet. Sci.* **30** 1933.

Elphic R. C., Lawrence D. J., Feldman W. C., Barraclough B. L., Maurice S., Binder A. B., and Lucey P. G. (1998) Lunar Fe and Ti abundances: Comparison of Lunar Prospector and Clementine data. *Science* **281,** 1493–1496.

Gillis J. J., Haskin L. A., and Spudis P. D. (1999) An empirical calibration to calculate thorium abundance from the Lunar Prospector gamma ray data. *Lunar Planet. Sci.* **30** 1699.

Gillis J. J., Jolliff B. J., Korotev R., and Lawrence D. J. (2000) An empirical relation between the Lunar Prospector gamma-ray and soil sample Th abundances. *Lunar Planet. Sci. Conf.* **31** 2058.

Gillis J. J. and Spudis P. D. (2000) Geology of the Smythii and Marginis region of the Moon: using integrated remotely sensed data. *J. Geophys. Res.* **105**(*E2*), 4217–4234.

Gillis J. J., Jolliff B. L., and Elphic R. C. (2003) A revised algorithm for calculation TiO_2 concentrations from Clementine UVVIS data: A synthesis of rock, soil, and remotely sensed TiO_2 concentrations. *J. Geophys. Res.* **108**(*E2*), 10.1029/2001JE0 01515.

Haskin L. A. and Warren P. H. (1991) Lunar chemistry. In *Lunar Sourcebook: A User's Guide to the Moon* (eds. G. Heiken, D. T. Vaniman, and B. M. French), pp. 357–474. Cambridge University Press.

Haskin L. A., Gillis J. J., Jolliff B. J., and Korotev R. L. (1999) On the distribution of Th in lunar surface materials. *Lunar Planet. Sci.* **30** 1858.

Haskin L. A., Gillis J. J., Korotev R. L., and Jolliff B. L. (2000) The materials of the lunar Procellarum KREEP Terrane: A synthesis of

data from geomorphological mapping, remote sensing, and sample analysis. *J. Geophys. Res.* **105**(*E8*), 20,403–20,416.

Hood L. L. and Jones J. H. (1987) Geophysical constraints on the lunar bulk composition and structure: A reassessment. *J. Geophys. Res.* **92**(Suppl.), E396–E410.

Jolliff B. L. (1999) Clementine UVVIS multispectral data and the Apollo 17 landing site: What can we tell and how well? *J. Geophys. Res.* **104**(*E6*), 14,123–14,148.

Jolliff B. L., Gillis J. J., Haskin L. A., and Korotev R. L. (2000) Major lunar crustal terranes: Surface expressions and crust-mantle origins. *J. Geophys. Res.* **105**(*E2*), 4197–4216.

Jolliff B. J. and Gillis J. J. (2002) Lunar crustal and bulk composition: Th and Al mass balance. In *Moon beyond 2002: Next Steps in Lunar Science and Exploration*, p. 29. LPI contribution No. 1128, Lunar and Planetary Institute, Houston.

Korotev R. L. (1998) Concentrations of radioactive elements in lunar materials. *J. Geophys. Res.* **103**(*E1*), 1691–1701.

Korotev R. L., Jolliff B. J., and Zeigler R. A. (2000) The KREEP components of the Apollo 12 regolith. *Lunar Planet. Sci.* **31** 1363.

Korotev R. L. and Gillis J. J. (2001) A new look at the Apollo 11 regolith and KREEP. *J. Geophys. Res.* **106**(*E6*), 12339–12354.

Korotev R. L., Jolliff B. L., Zeigler R. A., Gillis J. J., and Haskin L. A. (2003) Feldspathic lunar meteorites and their implications for compositional remote sensing of the lunar surface and the composition of the lunar crust. *Meteor. Planet. Sci.* **67**(*24*), 4895–4923.

Laul J. C. (1979) Neutron activation analysis of geologic materials. *Atomic Energy Rev.* **17**(3), 603–695.

Lawrence D. J., Feldman W. C., Barraclough B. L., Binder A. B., Elphic R. C., Maurice S., and Thomsen D. R. (1998) Global elemental maps of the Moon: The Lunar Prospector gamma-ray spectrometer. *Science* **281,** 1484–1489.

Lawrence D. J., Feldman W. C., Barraclough B. L., Binder A. B., Elphic R. C., Maurice S., Miller M. C., and Prettyman T. H. (2000) Thorium abundances on the lunar surface. *J. Geophys. Res.* **105**(E8), 20,307–20 331.

Lawrence D. J., Feldman W. C., Blewett D. T., Elphic R. C., Lucey P. G., Maurice S., Prettyman T. H., and Binder A. B. (2001) Iron abundances on the lunar surface as measured by the Lunar Prospector gamma-ray spectrometer. *Lunar Planet. Sci.* **32** 1830.

Lawrence D. J., Feldman W. C., Elphic R. C., Little R. C., Prettyman T. H., Maurice S., Lucey P. G., and Binder A. B. (2002) Iron abundances on the lunar surface as measured by the Lunar Prospector gamma-ray and neutron spectrometers. *J. Geophys. Res.* **107**(E12), 10.1029/2001JE0 01530.

Longhi J. and Ashwal L. D. (1985) Two-stage models for lunar and terrestrial anorthosites: Petrogenesis without a magma ocean. *Proc. Lunar Planet. Sci. Conf.* **9,** 79–99.

Lucey P. G., Spudis P. D., Zuber M. T., Smith D. E., and Malaret E. (1994) Topographic-compositional units on the Moon and the early evolution of the lunar crust. *Science* **266,** 1855–1858.

Lucey P. G., Taylor G. J., and Malaret E. (1995) Abundance and distribution of iron on the Moon. *Science* **268,** 1150–1153.

Lucey P. G., Blewett D. T., and Hawke B. R. (1998) Mapping the FeO and TiO_2 content of the lunar surface with multispectral imagery. *J. Geophys. Res.* **103**(*E2*), 3679–3699.

Lucey P. G., Blewett D. T., and Jolliff B. L. (2000) Lunar iron and titanium abundance algorithms based on final processing Clementine UVVIS images. *J. Geophys. Res.* **105**(*E8*), 20,297–20,305.

McEwen A. S., Eliason E., Lucey P. G., Malaret E., Pieters C. M., Robinson M. S., and Sucharski T. (1998) Summary of radiometric calibration and photometric normalization steps for the Clementine UVVIS images. *Lunar Planet. Sci.* **29** 1466.

Metzger A. E., Haines E. L., Parker R. E., and Radocinski R. G. (1977) Thorium concentration in the lunar surface. I: Regional values and crustal content. *Proc. Lunar Sci. Conf.* **8,** 949–999.

Nozette S. and The Clementine Team. (1994) The Clementine mission to the Moon: Scientific overview. *Science* **266,** 1835–1839.

Parker R. E., Haines E. L., and Metzger A. E. (1981) Potassium concetrations in the lunar surface. *Lunar Planet. Sci.* **12,** 811–812.

Prettyman T. H., Feldman W. C., Lawrence D. J., McKinney G. W., Binder A. B., Elphic R. C., Gasnault O. M., Maurice S., and Moore K. R. (2002) Library least squares analysis of Lunar Prospector gamma ray spectra. *Lunar Planet. Sci.* **33**, 2012.

Ringwood A. E. (1976) Limits on the bulk composition of the Moon. *Icarus* **28,** 325–349.

Staid M. I. and Pieters C. M. (2000) Integrated spectral analysis of mare soils and craters: Application to eastern nearside basalts. *Icarus* **145,** 122–139.

Taylor S. R. (1982) *Planetary Science: A Lunar Perspective*. Lunar and Planetary Institute.

Taylor S. R. and Jakes P. (1974) The geochemical evolution of the Moon. *Proc. Lunar Sci. Conf.* **5,** 1287–1305.

Taylor G. J., Hawke B. R., and Spudis P. D. (2002) Bulk composition of the Moon: Importance, uncertainties, and what we need to know. In *Moon beyond 2002: Next Steps in Lunar Science and Exploration*, p. 61. LPI contribution No. 1128, Lunar and Planetary Institue, Houston.

Toksöz M. N., Press F., Dainty A., Anderson K., Latham G., Ewing M., Dorman J., Lammlein D., Sutton G., and Duennebier F. (1972) Structure, composition, and properties of lunar crust. *Proc. Lunar Sci. Conf.* **3,** 2527–2544.

Warren P. (1994) Lunar and martian meteorite delivery services. *Icarus* **111,** 338–363.

Warren P. H. (2001) Compositional structure within the lunar crust as constrained by Lunar Prospector thorium data. *Geophys. Res. Lett.* **28,** 2565–2568.

Warren P. H. and Wasson J. T. (1979) Effects of pressure on the crystallization of a "chondritic" magma ocean and implications for the bulk composition of the Moon. *Proc. Lunar Sci. Conf.* **10,** 583–610.

Wieczorek M. A. and Phillips R. J. (1998) Potential anomalies on a sphere: Application to the thickness of the lunar crust. *J. Geophys. Res.* **103**(*E1*), 1715–1724.

Wieczorek M. A. and Zuber M. T. (2001) The composition and origin of the lunar crust: Constraints from central peaks and crustal thickness modeling. *Geophys. Res. Lett.* **28,** 4023–4026.

Wood J. A., Dickey J. S. Jr., Marvin U. B., and Powell B. N. (1970) Lunar anorthosites and a geophysical model for the Moon. In *Proceedings of the Apollo 11 Lunar Science Conference*, pp. 965–988. Pergamon Press.

York D. (1969) Least squares fitting of a straight line with correlated errors. *Earth Planet. Sci. Lett.* **5,** 320–324.